Research Article | Vol. 24, No. 22 | 31 Oct 2016 | OPTICS EXPRESS 25832

Optics EXPRESS

Investigation of solar noise impact on the performance of underwater wireless optical communication links

TASNIM HAMZA,[1,2,3] MOHAMMAD-ALI KHALIGHI,[1,4] SALAH BOURENNANE,[1] PIERRE LÉON[2], AND JAN OPDERBECKE[2]

[1]*Aix Marseille University, CNRS, Centrale Marseille, Institut Fresnel, Marseille, France*
[2]*IFREMER Research Institute, La Seyne-sur-Mer, France*
[3]*Tasnim.Hamza@fresnel.fr*
[4]*Ali.Khalighi@fresnel.fr*

Abstract: We investigate the effect of environmental noise, caused by solar radiations under water, on the performance of underwater wireless optical communication (UWOC) systems. Presenting an analytical and generic model for this noise, we examine its impact on the link performance in terms of the bit error rate (BER). This study is conducted for different photodetector types in the aim of highlighting practical limitations of establishing UWOC links in the presence of subsea solar noise. We show how the solar noise can impact the performance of UWOC links for relatively low operation depths. The results we present provide valuable insight for the design of UWOC links, which are likely to be established at relatively low depths. They can be exploited not only for the purpose of practical UWOC system deployment but also for in-pool experimental set-ups, since they elucidate the effect of ambient light on the measurements.

OCIS codes: (060.4510) Optical communications; (060.2605) Free-space optical communication.

References and links

1. M. A. Khalighi, C. Gabriel, T. Hamza, S. Bourennane, P. Léon, and V. Rigaud, "Underwater wireless optical communication; recent advances and remaining challenges," in *Proceedings of 16th International Conference on Transparent Optical Networks (ICTON)*, Graz, Austria, July 2014. pp. 1–4.
2. F. Hanson and S. Radic, "High bandwidth underwater optical communication," Appl. Opt. **47**(2), 277–283 (2008).
3. A. Fletcher, S. Hamilton, and J. Moores, "Undersea laser communication with narrow beams," IEEE Commun. Mag. **53**(11), 49–55 (2015).
4. C. Gabriel, M. A. Khalighi, S. Bourennane, P. Léon, and V. Rigaud, "Monte-Carlo based channel characterization for underwater optical communication systems," J. Opt. Commun. Netw. **5**(1), 1–12 (2013).
5. B. Cochenour, L. Mullen, and J. Muth, "Temporal response of the underwater optical channel for high-bandwidth wireless laser communications," IEEE J. Ocea. Eng. **38**(4), 730–742 (2013).
6. M. Doniec, M. Angermann, and D. Rus, "An end-to-end signal strength model for underwater optical communications," IEEE J. Ocea. Eng. **38**(4), 743–757 (2013).
7. F. R. Dalgleish, J. J. Shirron, D. Rashkin, T. E. Giddings, A. K. Vuorenkoski Dalgleish, I. Cardei, B. Ouyang, F. M. Caimi, and M. Cardeic, "Physical layer simulator for undersea free-space laser communications," Opt. Eng., **53**(5), 051410 (2014).
8. P. Lacovara, "High-bandwidth underwater communications," Marine Tech. Soc. J. **42**(1), 93–102 (2008).
9. S. Q. Duntley, "Light in the sea," J. Opt. Soc. Am. **53**(2), 214–233 (1963).
10. J. W. Giles and I. N. Bankman, "Underwater optical communication systems. part 2 : Basic design considerations," in *Proceedings of Military Communications Conference (MILCOM)* **3**, Atlantic City, NJ, USA (2005). pp. 1700–1705
11. J. E. Tyler, "Radiance distribution as a function of depth in an underwater environment," Bull. Scripps Inst. Oceanogr. **7**(5), 363–412 (1960).
12. C. D. Mobley, "A numerical model for the computation of radiance distributions in natural waters with wind-roughened surfaces," Limnol. Oceanogr. **34**(8), 1473–1483 (1989).
13. G. Cossu, R. Corsini, A. M. Khalid, S. Balestrino, A. Coppelli, A. Caiti, and E. Ciaramella, "Experimental demonstration of high speed underwater visible light communications," in *Proceedings of International Workshop on Optical Wireless Communications (IWOW)*, Newcastle upon Tyne, UK, Oct. 2013. pp. 11–15.
14. N. Farr, A. Chave, L. Freitag, J. Preisig, S. White, D. Yoerger, and P. Titterton, "Optical modem technology for seafloor observatories," in *Proceedings of OCEANS Conf.*, Boston, MA, 2006. pp. 1–6.
15. Sonardyne, `http://www.sonardyne.com/`.

#273319 http://dx.doi.org/10.1364/OE.24.025832
Journal © 2016 Received 9 Aug 2016; revised 4 Oct 2016; accepted 10 Oct 2016; published 28 Oct 2016

Optics EXPRESS

16. C. Mobley, *Light and Water: Radiative Transfer in Natural Waters* (Academic Press, 1994).
17. T. Petzold, *Volume Scattering Functions for Selected Ocean Waters* (Scri. Inst. of Ocean., 1972) San Diego, CA, USA.
18. Philips LUMILEDS Ligh. Co., *Luxeon rebel color portfolio datasheet ds68 20140527* (2014). http://www.lumileds.com.
19. J. M. Kahn and J. R. Barry, "Wireless infrared communication," Proceedings of IEEE **85**(2), 265–298 (1997).
20. R. Ramirez-Iniguez, S. M. Idrus, and Z. Sun, *Optical Wireless Communications: IR for Wireless Connectivity* (CRC Press, 2008).
21. M. Kavehrad, M. I. S. Chowdhury, and Z. Zhou, *Fundamentals of Optical Wireless Communications, in Short-Range Optical Wireless: Theory and Applications* (John Wiley and Sons, Ltd, 2015) Chichester, UK.
22. F. Xu, M. A. Khalighi, and S. Bourennane, "Impact of different noise sources on the performance of PIN- and APD-based FSO receivers," in *Proceedings of COST Action IC-0802 Workshop, IEEE ConTEL Conf.*, Graz, Austria, 2011. pp. 211–218.
23. R. Toledo-Crow, S. Shi, and Y. Li, "Analysis of a two-PMT system for simultaneous back- and forward-fluorescence detection in multiphoton microscopy," Biomedical Optics, OSA Technical Digest, BMD56.
24. B. E. A. Saleh and M. C. Teich, *Fundamentals of Photonics* (Wiley, 1991).
25. M. A. Khalighi, F. Xu, Y. Jaafar, and S. Bourennane, "Double-laser differential signaling for reducing the effect of background radiation in free-space optical systems," J. Opt. Commun. Netw. **3**(2), 145–154 (2011).
26. R. M. Gagliardi and S. Karp, *Optical Communications*, 2nd ed. (Wiley, 1995).
27. Hamamatsu, *Photomultiplier Tubes, Basics and Applications (Edition 3a)* (Hamamatsu Photonics K. K, 2007).
28. F. Qiang, *Encyclopedia of Atmospheric Sciences* (J. R. Holton, 2003), Chap. Radiation (solar). pp. 1859 – 1863.
29. ASTM-International, "Standard tables for reference solar spectral irradiances," http://www.astm.org/Standards/G173.htm.
30. T. Komine and M. Nakagawa, "Fundamental analysis for visible light communications using led lights," IEEE Trans. Consumer Elec. **50**(1), 100–107 (2004).
31. Hamamatsu, "R3896, R12896 High Sensitivity Multialkali Photocathode 28 mm (1-1/8 Inch) Diameter, 9-Stage, Side-On Type," http://www.hamamatsu.com.
32. W. C. Cox, "Simulation, Modeling and Design of Underwater Optical Communication Systems," (PhD Thesis, North Carolina University, Raleigh, North Carolina, USA, 2012).
33. ITU-T Recommendation G.975.1, (02/2004).
34. A. H. Azhar, T.-A. Tran, and D. O'Brien, "A Gigabit/s indoor wireless transmission using MIMO-OFDM visible-light communications," IEEE Photon. Technol. Lett. **25**(11), 171–174 (2013).
35. C. Mobley, E. Boss, and C. Roesler, *Ocean Optics Web Book* (2016). http://www.oceanopticsbook.info/
36. E. W. Abrahamson, Ch. Baumann, C. D. B. Bridges, F. Crescitelli, H. J. A. Dartnall, R. M. Eakin, G. Falk, P. Fatt, T. H. Goldsmith, R. Hara, T. Hara, S. M. Japar, P. A. Liebman, J. N. Lythgoe, R. A. Morton, W. R. A. Muntz, W. A. H. Rushton, T. I. Shaw, and J. R. Wiesenfeld, T. Yoshizawa , *Photochemistry of Vision* (Herbert J. A. Dartnall, 1972).
37. Z. Ghassemlooy, S. Rajbhandari, and W. Popoola, *Optical Wireless Communications: System and Channel Modelling with MATLAB* (CRC Press, 2013).

1. Introduction

Today we are witnessing an increasing interest in the exploration and exploitation of marine natural resources, which has raised demands for underwater wireless communications with much needed improved performance. One example is the deployment of underwater sensor networks and the need to data muling with the aid of autonomous underwater vehicles (AUVs) or remotely-operated vehicles (ROVs). Other typical scenarios include communication between AUVs or between an AUV and a submarine, e.g., for the purpose of docking or high rate data or multimedia transmission. It is well known that underwater wireless optical communication (UWOC) is a promising technology for such applications that allows establishing high data-rate, low-latency, and energy efficient communication links over distances of up to ~ 150 m typically in clear waters [1–3]. In a previous work [4], we studied the UWOC channel and showed that in low-to-moderate turbidity waters the channel delay dispersion is practically negligible and concluded that, under such conditions, the channel can effectively be considered as frequency non-selective, i.e., not introducing inter-symbol interference. This fact has been confirmed by several other studies so far, see for instance [5, 6].

We focus in this work on the effect of the background noise generated by solar radiations on

Optics EXPRESS

the communication link performance. In fact, the effect of the solar noise has been neglected in most previous works in the literature. The assumption of negligible background noise is rational only when working in large operation depths, where the aquatic channel can effectively be considered as dark [8]. To the best of our knowledge, the accuracy of this assumption has not been examined so far for the case of relatively low depths, typically less than a few hundreds of meters. Indeed, due to high water transparency in the case of clear ocean waters, the blue-green wavelengths of light can deeply penetrate in water, which can be detected using sensitive detectors even at depths larger than 600 m [9].

Nevertheless, a few works have initiated studying the impact of the background noise. For instance, in [10], the authors presented some general considerations for the design of UWOC systems and enumerated the different noise sources affecting the receiver. They considered *inter alia* the effect of background noise generated by ambient light on the system performance and provided the expression of the resulting shot noise as a function of upwelling solar radiance in (W m^{-2} sr^{-1}). However, the computation of this parameter depends on several factors for which exhaustive measurements are not available, to the best of our knowledge. In [11] and [12], Tyler and Mobley presented the measured solar radiance distribution underwater but unfortunately their data were limited to relatively low depths, i.e., smaller than 60 m. On the other hand, p-resenting a preliminary study, Lacovara reported in [8] that background noise would generally limit the communication range by almost 20 m, without specifying the receiver opto-electronic components, e.g. the photo-detector (PD) type nor the transmission conditions. Lastly, in [13], Cossu *et al.* carried out an experimentation under summer sunlight illumination and achieved a 'potentially error-free' UWOC transmission up to 58 Mbps over a 2.5 m range. However, although data acquisition was undertaken in the presence of sunlight, the resulting noise effect on the link performance was not identified precisely.

In this paper, we present an analytical generic model of the solar noise and study its impact on the UWOC link performance in terms of bit-error rate (BER). Our study considers three different PD types, i.e., PIN, avalanche photo-diode (APD), and photo-multiplier tube (PMT), in order to highlight the practical limitations of establishing an UWOC link for each case. Meanwhile, we take into account the characteristics of the other link components, such as the emitting source radiation pattern and power spectrum at the transmitter (Tx), the optical filter at the receiver (Rx), as well as the Rx field-of-view (FOV) and aperture size. We show that solar noise can strongly limit the BER performance of the UWOC link for relatively low depths, around several hundreds of meters for the case of a PMT or several tens of meters for a PIN PD. In the numerical results that we present, we consider some special assumptions on the properties of the solar radiations, link configuration, and water turbidity. Nevertheless, the main results that we present are quite insightful for the design of UWOC links that are likely to be established at relatively low depths.

The remainder of the paper is organized as follows. In Section 2, we present the UWOC system description including channel model and the Rx electrical noise for the three PD types. Next, the details on background solar noise modeling are provided in Section 3. Then, in Section 4, we present some numerical results to evaluate and quantify the impact of solar noise on the UWOC link performance. Lastly, Section 5 concludes the paper.

2. Main assumptions and system model

Let us consider a point-to-point communication link represented in Fig. 1. The Tx is assumed to use a light-emitting diode (LED), which has the advantages of low cost, high power, and relatively wide beam, compared to a laser diode. Note that the use of a relatively wide beam facilitates the pointing and beam alignment issues. At the Rx, after photo-detection and trans-impedance amplification, the signal is low-pass filtered to limit the Rx noise, and then time-sampled prior to data detection to retrieve the transmitted bits. We consider three types of PDs,

Optics EXPRESS

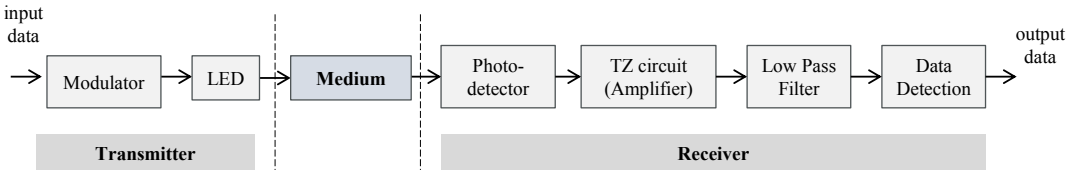

Fig. 1. End-to-End general Block Diagram of UWOC communication link.

i.e., PIN, APD, and PMT. Whereas PIN PD is the 'classical choice,' APDs are interesting due to their inherent gain and have been considered in several previous experimental and theoretical works, e.g. [5, 6, 13]. PMTs, on the other hand, are low noise and have high sensitivity and gain, typically with a high bandwidth and a relatively large aperture, compared to semiconductor counterparts. They have also been considered in several previous theoretical works such as [2, 5, 14] and also recently used in the BlueComm modem, developed by Woods Hole oceanographic institution (WHOI) and commercialized by Sonardyne, for instance [15]. Meanwhile, they are larger and more expensive, require high voltage for operation, are more easily damaged from exposure to high-intensity light, and have a limited dynamic range [8]. Note that our aim here is not to compare the relevance of using one PD type or another, but rather to focus on the impact that the solar background noise can have on the link performance when these components are used at the Rx, and the general trend of the dependency of the link performance on the Rx operation depth.

2.1. Underwater optical channel

The propagation of light under water is governed by the water optical properties [9]. Light can be subject to significant absorption and scattering due to its interaction with water molecules and dissolved particles, depending on both wavelength λ and water turbidity [16]. In this paper, we consider $\lambda = 532$ nm, which presents relatively low attenuation rates for low-turbidity waters [16]. Without loss of generality, we conduct our study for the case of clear ocean waters with the typical Chlorophyll concentration of $0.5\,\mathrm{mg/m^3}$ [17].
For the sake of simplicity and in order to focus on the effect of solar noise, we model the power loss by the exponential decay model. This way, denoting the link span by Z, the channel loss L_{ch} is given by:

$$L_{\mathrm{ch}} = \exp(-K\,Z), \tag{1}$$

where K is the diffuse attenuation coefficient, see Section 3. This model is better adapted to the case of a LED emitter that cannot be considered as a collimated beam but rather a diffuse source, see [10].

2.2. Optical source power distribution

As mentioned previously, we consider an LED-based Tx, and without loss of generality, we model the LED radiation pattern by a generalized Lambertian model with azimuthal symmetry [18] as follows:

$$P(\phi) = P_{\mathrm{Tx}}\,\frac{m+1}{2\pi}\cos^{m}(\phi) \quad [\mathrm{W/sr}], \tag{2}$$

where P_{Tx} denotes the total emitted Tx power, $\phi \in [0, \pi/2]$ is the angle of irradiance, and m stands for the Lambertian order, given by $m = -\ln(2)/\ln(\cos(\phi_{1/2}))$, with $\phi_{1/2}$ being the Tx semi-angle at half-power.

Optics EXPRESS

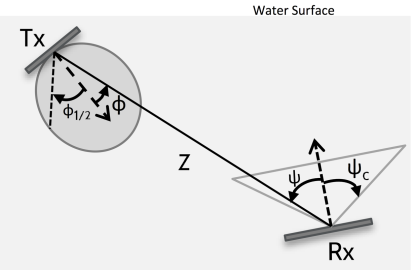

Fig. 2. Illustration of the considered UWOC system and the related parameters.

2.3. Receiver optics considerations

The Rx employs a bandpass optical filter in order to attenuate the ambient light, i.e., background noise level. We denote by $T_s(\psi)$ the average filter transmission over the filter wavelength range $\Delta\lambda$ (i.e., filter bandwidth) for a specific angle of incidence ψ. We also consider an optical concentrator of gain $g(\psi)$, employed in order to increase the Rx effective area of light collection, A_{eff}. We have [19]:

$$A_{\text{eff}}(\psi) = \begin{cases} A_{\text{PD}}\, T_s(\psi)\, g(\psi)\, \cos(\psi), & 0 \leqslant \psi \leqslant \psi_c \\ 0, & \psi > \psi_c \end{cases} \tag{3}$$

where A_{PD} is the physical area of the PD, ψ is the angle of incidence, and ψ_c denotes the FOV (semi-angle) of the concentrator. We assume an idealized non-imaging concentrator [19], which provides a gain of:

$$g(\psi) = \begin{cases} \frac{n^2}{\sin^2(\psi_c)}, & 0 \leqslant \psi \leqslant \psi_c \\ 0, & \psi > \psi_c \end{cases} \tag{4}$$

where n is its internal refractive index. The advantage of using a non-imaging over an imaging concentrator is that it offers a higher FOV and therefore more flexibility regarding beam misalignments [20]. Note that by this model, we assume that the light received in the concentrator FOV is totally captured by the PD, i.e., neglect any limitation of the Rx FOV that could be caused by the PD.

2.4. Received optical power

Let us consider the Rx and Tx configuration illustrated in Fig. 2. Assuming perfect Tx-Rx alignment, the channel DC gain is given by [19, 21]:

$$H(0) = \begin{cases} \frac{m+1}{2\pi} \cos^m(\phi)\, \frac{A_{\text{PD}}}{Z^2}\, T_s(\psi)\, g(\psi)\, \cos(\psi), & 0 \leqslant \psi \leqslant \psi_c \\ 0, & \psi > \psi_c \end{cases} \tag{5}$$

where Z is the distance separating the Tx and the Rx, and ϕ and ψ are the Tx and Rx offset angle relative to the optical axis (i.e., the line-of-sight), respectively. Then, the received optical power P_{Rx} can be expressed as function of emitted power P_{Tx} as follows:

$$P_{\text{Rx}} = H(0)\, L_{\text{ch}}\, P_{\text{Tx}}. \tag{6}$$

Optics EXPRESS

2.5. Receiver electrical noise

In [22], Xu *et al.* provided a complete model for the Rx noise in terrestrial free-space optical communication systems. We use the main results of this paper in order to model the Rx electrical noises for the three cases of PIN, APD and PMT detectors within our context. We reasonably neglect the dark current noise assuming a Silicon (Si) PD for the case of PIN and APD [22, 23] and take into account the Rx thermal noise (mainly arising from the trans-impedance amplifier) and the photo-current shot noise, arising from input signal and/or background radiations.
The Rx thermal and shot noise are classically modeled by a zero-mean Gaussian and a Poisson random process, respectively. Concerning the latter, when the signal power or background radiations are of relatively high level, the corresponding average number of received photons is large enough so as to approximate the Poisson distribution by a Gaussian one [24] (obviously, this is not the case when working with very low signal levels where the Poisson model has to be used, as shown in [7]). The corresponding mean value is rejected by the ac-coupled receiver circuitry, therefore, the zero-mean Gaussian model also applies to the shot noise component [25]. The Gaussian model remains valid for the case of using an APD or similarly a PMT at the receiver (see [22] for more detail). Note that the square-law characteristic of the PD does not put into question this modeling. As we have shown in a previous work [22], the contributions from the interaction of the signal with background radiations due to this non-linear characteristic of the PD can be practically neglected.

Without loss of generality, we assume intensity modulation with direct detection (IM/DD), based on on-off keying (OOK), which has the advantage of implementation simplicity. Then, globally, the PD output current distribution is approximated by a Gaussian process that we denote by $\mathcal{N}(\mu_0, \sigma_0^2)$ and $\mathcal{N}(\mu_1, \sigma_1^2)$ corresponding to off and on OOK symbols, respectively. Let us denote by I the average photo-current generated by the PD, composed of signal (I_s) and noise (I_b) parts, that is, $I = I_\mathrm{s} + I_\mathrm{b}$. We have [22]:

$$\left\{ \begin{array}{lcl} \mu_0 & = & I_\mathrm{b} \\ \sigma_0^2 & = & 2e\,G\,F\,I_\mathrm{b}\,B + \frac{4KTB}{R_\mathrm{L}} \end{array} \right. \tag{7}$$

$$\left\{ \begin{array}{lcl} \mu_1 & = & I_\mathrm{s} + I_\mathrm{b} \\ \sigma_1^2 & = & 2e\,G\,F\,(I_\mathrm{s} + I_\mathrm{b})\,B + \frac{4KTB}{R_\mathrm{L}} \end{array} \right. \tag{8}$$

Here, e, K, T, B, and R_L denote the electron charge, the Boltzmann constant, the temperature in Kelvin, the Rx low-pass filter bandwidth, and the load resistance of the trans-impedance (TZ) amplifier, respectively (note that we have neglected the internal TZ amplifier noise assuming implicitly that a low-noise amplifier is used with noise figure close to one). Also, G is the PD internal amplification gain, which is equal to one for a PIN PD. We denote this parameter by G_APD and G_PMT for the cases of APD and PMT, respectively. For the latter case, we have $G_\mathrm{PMT} = \alpha\,\delta^{n_\mathrm{d}}$, where δ denotes the PMT secondary emission ratio, n_d stands for the number of dynodes (multiplication stages), and α is the collection efficiency of the first dynode [27]. In addition, F is the PD noise figure, where $F = 1$ for a PIN PD, $F = \xi G_\mathrm{APD} + (2 - 1/G_\mathrm{APD})(1 - \xi)$ for an APD with ξ being its ionization ratio [22], and $F = \delta/(\delta - 1) \approx 1$ for a PMT [27]. Lastly, we have, for instance, $I_\mathrm{b} = \eta\,G\,P_\mathrm{b}\,e/\hbar\,\nu$, where P_b denotes the optical power of the background radiations, and $\hbar$ and ν denote the Planck constant and the wave frequency, respectively.

3. Solar noise modeling

In order to quantify the amount of solar irradiance captured by the Rx and its effect on the system performance, we consider the solar spectral downwelling plane irradiance that we denote by $E_\mathrm{sun}(\lambda, D)$ in $\mathrm{W\,m^2\,nm^{-1}}$, where λ and D denote the wavelength and the operation depth (i.e., the depth at which the Rx platform is positioned), respectively. Measurements of E_sun at

Optics EXPRESS

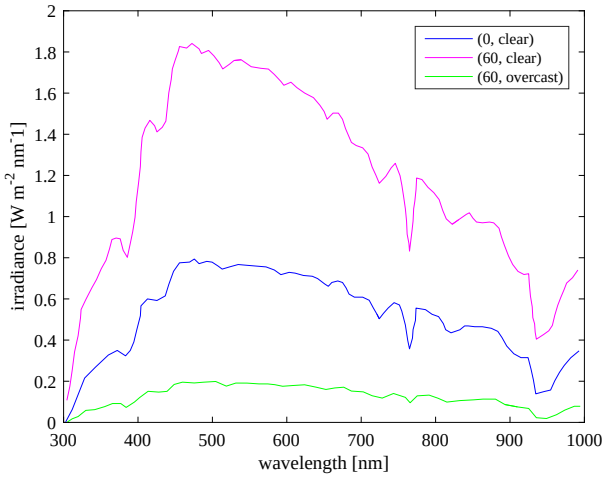

Fig. 3. Sea-level solar spectral irradiance for different combinations of sun zenith angle and atmospheric conditions (reproduced from [35]).

the sea level (i.e., at $D = 0$) can be found for instance in [35]. We have reproduced a part of these data in Fig. 3, where we notice an important difference between the presented irradiance plots, showing the strong dependence of E_{sun} on the weather conditions and sun positions (i.e., sunlight angle with respect to the zenith). Although these data do not describe the general case, using them allows us to approximate the Rx noise arising from solar radiations and therefore get an estimate of their effect on the system performance. In addition, these data are consistent with the measurements of the solar power spectral density by the American society for testing and material (ASTM) presented in [28].

Here, in order to investigate the worst impact of the solar noise on the Rx performance, we consider the case of the clear weather where the sun is located at the zenith. Under these conditions, E_{sun} reaches its peak value, as can be seen from Fig. 3, which is around $0.7645\,\text{W}\,\text{m}^2\,\text{nm}^{-1}$ for $\lambda = 532\,\text{nm}$.

When the sunlight penetrates in water, it becomes increasingly diffuse and attenuates exponentially with the depth D. This assumption is consistent with the depth profiles of underwater irradiance presented in [9]. Thus, we characterize the solar power decay underwater by the spectral diffuse attenuation coefficient K (which is a function of λ) for spectral downwelling plane irradiance as follows:

$$E_{\text{sun}}(\lambda, D) = E_{\text{sun}}(\lambda, 0)\ \exp(-K\,D), \tag{9}$$

where we implicitly assumed that K is almost independent of D, which is rational for the case of homogeneous waters [36]. In practice, K does depend on D and its variations have to be taken into account, although it converges to an asymptotic value for depths higher than 60 m, see [9] for experimental depth profiles of K. However, the precise mathematical modeling of K is out of the scope of this work. That is why, for the sake of simplicity, we assume that K is almost constant for the considered range of D, and take the pessimistic (lowest) corresponding values of K, see Fig. 24 in [9]. Therefore, considering the case of clear ocean waters corresponding to a Chlorophyll concentration of $C \approx 0.5\,\text{mg}\,\text{m}^{-3}$ (Jerlov type II water), we estimate K based on the bio-optical model provided by Morel in [16], which gives $K \approx 0.08\,\text{m}^{-1}$ for $\lambda = 532\,\text{nm}$.

Let us consider the case study illustrated in Fig. 4, where α denotes the Rx inclination angle with respect to the zenith. The solar radiations captured by the PD generate an average photo-

Optics EXPRESS

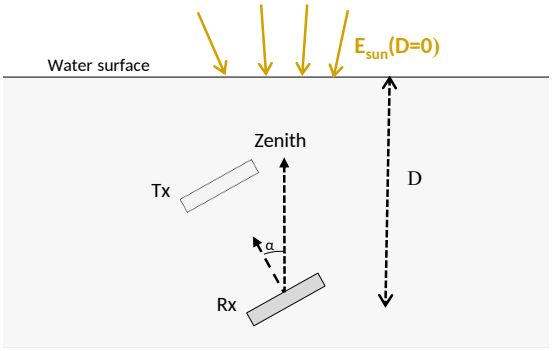

Fig. 4. Illustration of the considered Sun and UWOC system configuration with the related position parameters.

current I_b and a random component of variance $\sigma_b^2 = 2\,e\,G\,F\,I_b\,B$, see Subsection 2.5. In order to calculate I_b, we should first estimate the optical power P_b of the solar noise captured at the Rx. Using E_{sun}, we can evaluate the sunlight irradiance (in W/m^2) within the bandwidth $\Delta\lambda$ of the Rx optical filter. We assume that the Rx light collecting surface captures the solar irradiance according to the cosine law [36]. We further assume that there is no effect of obstruction or spatial filtering at the Rx side to limit the solar irradiance (this can be considered as a worst case). Then, P_b can be calculated as follows.

$$P_b = \begin{cases} E_{sun}(D)\,t\,\Delta\lambda\,\exp(-K\,D)\,A_{eff}\,\cos(\alpha), & 0 \leqslant \alpha \leqslant \psi_c \\ 0, & \alpha > \psi_c \end{cases} \tag{10}$$

Here, t is the water transmittance that is set to $t \approx 95\%$ for $\lambda = 532$ nm, based on the experimental data presented in [35] (although this value depends on the experiment conditions in [35], this could be considered as a typical value). Lastly, note that in Eq. (10), we implicitly assumed that the solar irradiation spectral density underwater is constant over the considered Rx optical filter bandwidth $\Delta\lambda$ (typically on the order of several nm to several tens of nm), which is a fair approximation in practice [8].

4. Numerical results

We present in this section some numerical results in order to quantify the impact of solar noise on the performance of a typical UWOC link operating in clear ocean waters. The rationality of this choice of water type is that background light can have its most significant impact on the link performance in clear waters, where it can penetrate in larger depths [8]. In fact, given the considered link configuration, although for higher turbidity waters we have a more significant contribution of multiple scattering effect in the received ambient light intensity at the Rx, the high channel loss due to absorption and scattering has a more dominant effect and makes the link less susceptible to solar noise, compared to the case of clear waters. Nevertheless, more in-depth investigation would be necessary for the case of a horizontal link.
We further assume perfect beam alignment and time synchronization between the Tx and the Rx. Data transmission is performed according to uncoded OOK signaling.

4.1. Parameter specification

The considered Tx and Rx parameters are specified in Table 1. Here, $R = 10$ Mbps is the data transmission rate, which can be readily attained using the typical off-the-shelf available LEDs (for instance, LUXEON Rebel Color components [18]). The LED is considered to emit at the

Optics EXPRESS

wavelength $\lambda = 532$ nm with a Lambertian order of 20, resulting in $\phi_{1/2} \approx 15°$. We assume that the three PD types, i.e., PIN, APD, and PMT, have equal surfaces and quantum efficiencies. We also consider the bandwidth of $\Delta\lambda = 30$ nm for the passband optical filter that matches the LED spectral width [18] and, for the sake of simplicity, assume that $T_s(\psi) \approx 1$ [30].

Table 1. Tx-Rx parameter specification

(a) Tx

Parameter	Value
λ	532 nm
$\Delta\lambda$	30 nm
P_{Tx}	100 mW
$\phi_{1/2}$	15 °
R	10 Mbps

(b) Rx

Parameter	Value
η	0.82
R_{L}	50 Ω
$\Delta\lambda$	30 nm
G_{APD}	50
ξ	0.02 (for APD)
n_{d}	9 (PMT) [31]
δ	6 (typical PMT) [27]

We have not specified the Rx FOV ψ_{c} and A_{PD} in the table because as it can be seen from Eq. (10), the optical power P_{b} of the solar radiations captured at the Rx depends on both of these parameters. Therefore, in our performance study we will later consider a range of values for ψ_{c} and A_{PD} of practical relevance in order to describe various Rx configurations. The considered values of the Rx FOV and aperture size are presented in Tables 2 and 3, where $A_{\mathrm{PD}} = \pi\, d_{\mathrm{PD}}^2/4$. It is worth mentioning that the receiver filters corresponding to the largest FOVs specified in Table 2 may not be practically realizable or will be very expensive, in particular, given the 30 nm filter bandwidth that we assumed, see Table 1(b). However, we consider these values here for the sake of completeness of our study. On the other hand, in Table 3, the smallest aperture sizes correspond to the typical available PD devices (e.g. by Hamamatsu). The largest d_{PD} values, however, are less relevant for PIN and APD devices, given the relatively high data rate of 10 Mbps considered here. Nevertheless, considering these values is interesting as this allows to see the ultimate effect of the aperture size [32].

Table 2. Simulated Rx FOVs

FOV	0.5°	1°	2°	4°	8°	16°	45°

Table 3. Simulated Rx aperture diameters

d_{PD}	5 mm	10 mm	1 in	2 in	3 in	4 in

4.2. System performance in the absence of solar noise

In order to have a benchmark in our study of the impact of solar background noise on the performance of an UWOC link, we start by evaluating the system BER in the absence of solar noise. We conduct this study for the three PD cases described in Section 2.5. Note that our main goal is not to compare the performances of these PDs but rather to have a benchmark of their respective performances, useful for further investigations. We have presented in Fig. 5 the variations of BER versus link range Z, independently of the operation depth D (which does not influence the system performance in the present study), and for different values of the Rx FOV

Optics EXPRESS

ψ_c and aperture diameter d_{PD} (calculating the Rx SNR for each Z, the BER for uncoded OOK can be readily calculated [37]).

4.2.1. Effect of Rx FOV

We first fix the Rx aperture to $d_{PD} = 5$ mm and investigate the effect of changing the Rx FOV ψ_c. (This d_{PD} corresponds to the smallest PD size in Table 3 but is typical of available PIN and APD devices.) Results are shown in Figs. 5(a), 5(c) and 5(e), for PIN-, APD-, and PMT-based receivers. The dotted horizontal lines correspond to BER $= 10^{-4}$ that we consider as target BER. Note that a *raw* BER of 2×10^{-3} is usually considered as sufficiently low for an uncoded system, which can readily be reduced to less than 10^{-9} by employing error correction coding [33] (see [13,34], for instance). For the three considered PDs, we notice an improvement in terms of maximum achievable link distance when ψ_c is reduced. Indeed, varying ψ_c form 45° to 0.5° allows an increase in the link span of about 50, 70, and 87 m, for the cases of using the PIN, APD and PMT, respectively. This increase in the link span is in fact due to the increase in the optical concentrator gain $g(\psi)$ by reducing the Rx FOV, see Eq. (4) (remember that in this section we assume the absence of solar noise). Considering $\psi_c = 0.5°$, we notice the maximum link range of 57, 93, and 147 m for PIN-, APD-, and PMT-based receivers, respectively, for a target BER of 10^{-4}. This illustrates the significant performance improvement when using a PMT, compared to PIN or APD, as expected. Notice that such a comparison is relevant because all the three PD types were assumed to have the same active area.

4.2.2. Effect of Rx aperture size

Let us now fix the Rx FOV to $\psi_c = 16°$ and see the impact on the performance by varying d_{PD}. (Such a moderate Rx FOV would make a good compromise between facilitating link alignment and minimizing geometric optical power loss.) Simulation results are presented in Figs. 5(b), 5(d) and 5(f), for PIN, APD, and PMT cases, respectively. As expected, the maximum achievable link distance increases as the Rx aperture increases, since the captured intensity by the Rx is proportional to its collection area. Indeed, varying d_{PD} form 5 mm to 101.6 mm (4 inch), allows a distance gain of 38, 52, and 61 m, for the cases of PIN, APD, and PMT, respectively.
It is worth mentioning that the largest PD sizes may be considered as irrelevant from a practical point of view. Especially, considering these values assumes that we are not concerned by the practical fabrication issues of the corresponding non-imaging concentrator. That is to say, we implicitly assume that we have adapted concentrator and optics to the PD size.

4.3. Impact of solar background noise

Now let us investigate the impact of background noise on the system performance. Our aim is first to elucidate the effect of solar radiations when using different PD types, and secondly to identify the conditions under which the assumption of neglecting the solar noise is rational.

4.3.1. Simulation parameters and assumptions

Because solar rays' power is attenuated as they penetrate in water, we study the BER performance as a function of the operation depth that we define as the Rx depth D. Considering a target BER of 10^{-4} in the absence of solar noise, we fix the link range Z for each PD type, and investigate the variations of BER as a function of D in the presence of solar noise. We have provided the corresponding link spans Z for different values of the Rx FOV and aperture diameter in Tables 4 and 5, respectively. To study the impact of the solar noise, we consider the worst case configuration where the sun is at the zenith. This corresponds to the peak value of E_{sun} (see Section 3 and Fig. 3). We further assume that the Rx plan is directed towards the sea surface, i.e., we set $\alpha = 0°$, generating a maximum of captured solar irradiation, see Eqs. (3)-(6) and Fig. 2. Note that although this assumption, as well as that of the absence of spatial filtering

Optics EXPRESS

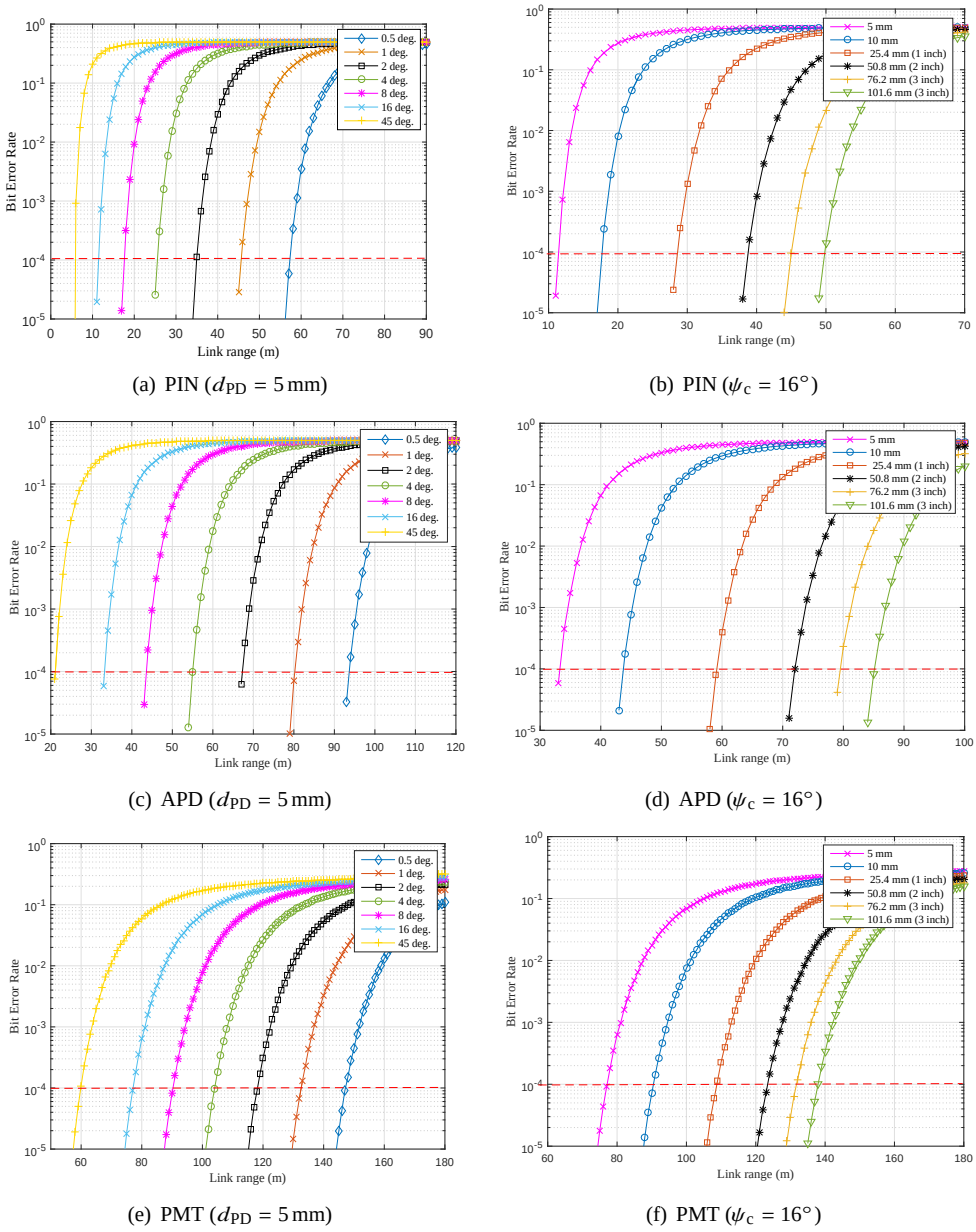

(a) PIN ($d_{\mathrm{PD}} = 5\,\mathrm{mm}$)

(b) PIN ($\psi_{\mathrm{c}} = 16°$)

(c) APD ($d_{\mathrm{PD}} = 5\,\mathrm{mm}$)

(d) APD ($\psi_{\mathrm{c}} = 16°$)

(e) PMT ($d_{\mathrm{PD}} = 5\,\mathrm{mm}$)

(f) PMT ($\psi_{\mathrm{c}} = 16°$)

Fig. 5. BER performance as a function of link range Z for PIN-, APD-, and PMT-based receivers in the absence of solar noise. P_{Tx}= 0.1 W, uncoded OOK modulation, Jerlov type II waters with Chlorophyll concentration of $C = 0.5\,\mathrm{mg.m}^{-3}$. Two cases of fixed Rx aperture size and fixed Rx FOV (left and right sub-figures, respectively) are considered.

or obstruction, are not likely to happen in practice, this worst case study determines the maximum limitation on the system performance. In other words, for a set of system parameters, the specified 'pessimistic' noise-free depth will be valid for any system configuration and operation scenario. Nevertheless, the case of vertical links is typical, for instance, in the case of data upload from an AUV to a ship or a submarine, or in the case of data-muling by an AUV or an

Optics EXPRESS

ROV.

Table 4. Link span Z(m) satisfying BER $\approx 10^{-4}$ for different Rx FOVs ψ_c in the absence of solar noise, $d_{PD} = 5$ mm.

FOV	0.5°	1°	2°	4°	8°	16°	45°
PIN	57.1	45.4	34.9	25.3	17.3	11.1	5.6
APD	93.5	80.1	67.2	55.0	43.4	33.1	21.0
PMT	147.2	132.5	118.1	104.0	90.2	77.1	59.9

Table 5. Link span Z(m) satisfying BER $\approx 10^{-4}$ for different Rx aperture diameters d_{PD} in the absence of solar noise, $\psi_c = 16°$.

d_{PD}	5 mm	10 mm	1 inch	2 inch	3 inch	4 inch
PIN	11.1	17.4	28.3	38.6	45.0	49.7
APD	33.1	43.5	59.1	72.0	79.3	85.1
PMT	77.1	90.4	108.7	123.3	131.7	137.9

4.3.2. Solar noise impact as a function of Rx FOV

We have presented in Figs. 6(a), 6(c) and 6(e) simulated BER results as a function of the Rx depth D for $d_{PD} = 5$ mm and the three PD types and different values of the Rx FOV. Note that the link span Z varies depending on the PD type and ψ_c, see Table 4. These figures illustrate the role of the Rx depth in the performance degradation caused by the solar noise. As expected, the Rx BER performance strongly deteriorates in relatively small depths. For instance, considering a small FOV of $\psi_c = 0.5°$, the BER approaches 10^{-1} at depths around 80, 190, and 325 m, for the cases of PIN, APD, and PMT, respectively. The BER converges to the target value of $\sim 10^{-4}$ (in the absence of background noise) for depths larger than about 140, 250, and 400 m for PIN, APD, and PMT cases, respectively. Given that we are considering the worst case configuration concerning the solar noise effect, we can for sure neglect the the solar background noise effect for depths larger than these values, whatever the transmission scenario. Here, reasonably, PMTs are more sensitive to background noise than APD or PIN PD.

Furthermore, we notice that increasing the Rx FOV makes the Rx performance less vulnerable to background noise. For instance, if we increase ψ_c form 0.5° to 45°, the minimum depth at which the target BER can be attained decreases by ~ 100 m for the three PD cases. In other words, by increasing the Rx FOV, the link performance is less affected by the background noise. This finding may seem strange since one may expect that a larger FOV should rather result in more collected solar radiations at the Rx, and hence, should impact more significantly the Rx performance. To explain this behavior, firstly remember that for the different FOV values considered here, the signal level is kept as constant (the corresponding links spans can be found in Table 4). Secondly, remember that we are considering the use of a non-imaging concentrator at the Rx, for which a larger FOV corresponds to a smaller concentrator gain, see Eq. (4). This, in turn, results in a reduction of the intensity of the background radiations captured at the Rx.

4.3.3. Solar noise impact as a function of Rx aperture size

We have presented the simulated BER results in Figs. 6(b), 6(d) and 6(f), for $\psi_c = 16°$ and different PD diameters, considered in Table 3. Remember that the corresponding link spans Z

Optics EXPRESS

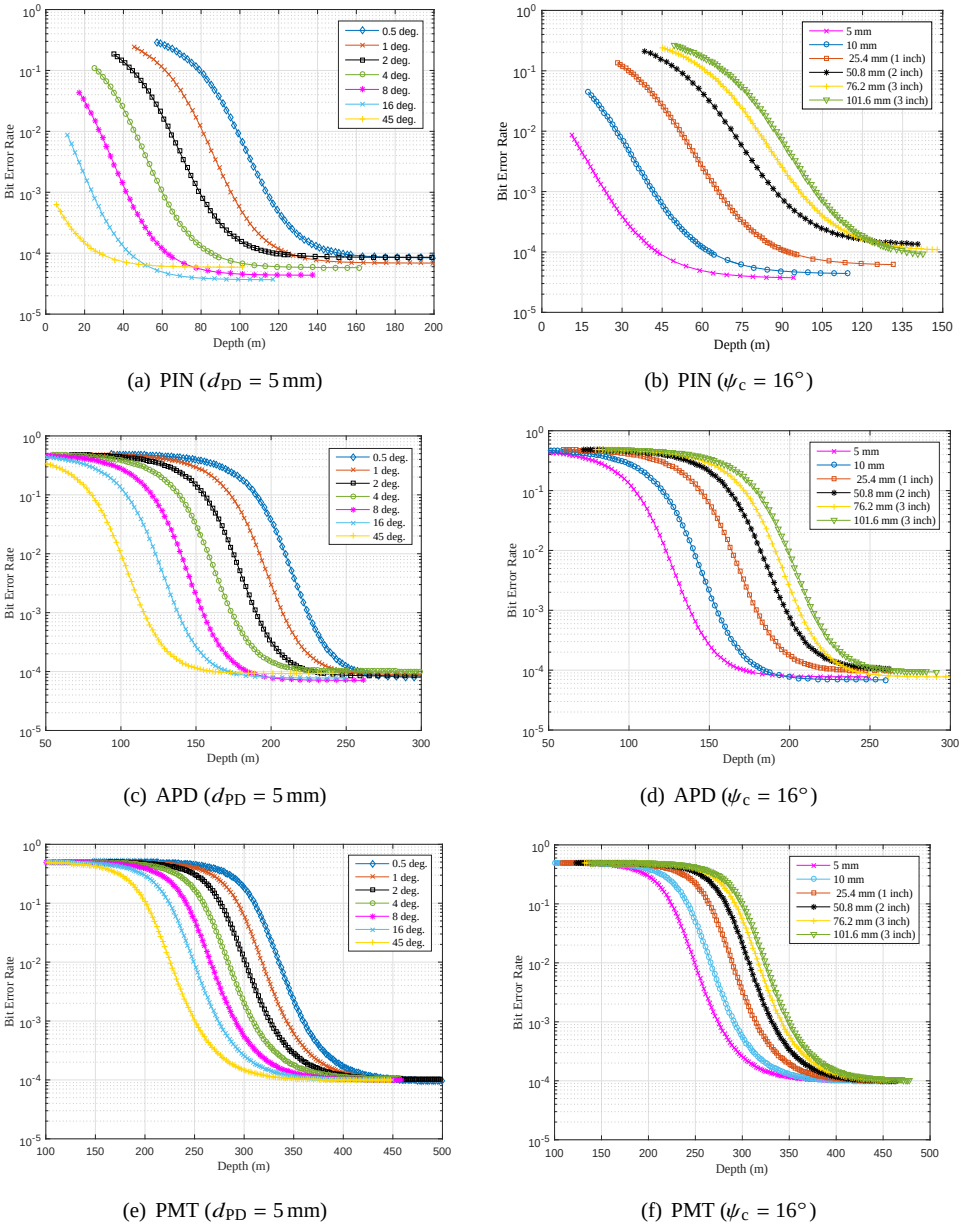

(a) PIN ($d_{\mathrm{PD}} = 5\,\mathrm{mm}$)

(b) PIN ($\psi_{\mathrm{c}} = 16°$)

(c) APD ($d_{\mathrm{PD}} = 5\,\mathrm{mm}$)

(d) APD ($\psi_{\mathrm{c}} = 16°$)

(e) PMT ($d_{\mathrm{PD}} = 5\,\mathrm{mm}$)

(f) PMT ($\psi_{\mathrm{c}} = 16°$)

Fig. 6. Impact of solar noise on the BER performance as a function of the Rx depth D for PIN-, APD-, and PMT-based receivers. $P_{\mathrm{Tx}} = 0.1\,\mathrm{W}$, uncoded OOK modulation, Jerlov type II waters with Chlorophyll concentration of $C = 0.5\,\mathrm{mg.m}^{-3}$. Two cases of fixed Rx aperture size and fixed Rx FOV (left and right sub-figures, respectively) are considered.

depend on d_{PD} and the PD type, see Table 5. We notice that, unlike the FOV, when the Rx aperture increases, the depth limit under which the Rx performance is not affected by the background noise, increases. Indeed, varying d_{PD} from 5 mm to 4 inch increases the depth limit by $\sim$ 80 m for the three PD cases. In other words, for increased PD size, the link performance is affected more considerably by the background noise. This is explained by the fact that the

Optics EXPRESS

captured solar radiation intensity is proportional to the Rx collection area, assuming an ideal non-imaging concentrator, see Eqs. (3) and (10). Overall, for different link configurations, we can deduce from these results the minimum depth at which the communication can take place without being effectively impacted by the solar background noise.

5. Conclusions and discussions

In this work, we investigated the potential impact of solar background noise on the performance of point-to-point UWOC links for different types of PDs, i.e., PIN, APD, and PMT. Considering an accurate model for the received solar noise at the Rx, we presented through numerical results a comprehensive study of the noise effect on the system performance for different Rx parameters. In particular, we showed how the sensitivity to solar radiations varies depending on both the operation depth and the Rx characteristics. Indeed, for relatively low depths (typically less than 80 m), a PIN-based Rx has more robustness against the background noise, compared to APD- and PMT-based receivers. This latter was shown to be very sensitive to solar radiations and should be used in receivers working at relatively large operational depths, i.e., more than 200 m. The results we presented are insightful for UWOC system designers and also users when these links have to be deployed in relatively shallow waters where the propagation medium cannot be considered as dark.

The real impact of the background noise on the Rx performance depends on a number of parameters, including the sun position and its radiation intensity, the direction of the Rx as well as its aperture size and FOV, the type of Rx concentrator, the spectral/spatial response of the Rx optical filter, etc. Studying the effect of each parameter regarding the received solar noise on the PD would not be practically useful and exploitable. Therefore, in the presented simulation results, we considered the worst case for the link configuration where the maximum of the solar radiations was captured by the Rx, although such a case may rarely happen in practice. Nevertheless, the interest of studying this worst case is that the *pessimistic* limits that we provided for the effectively noise-free operation will apply to any other link configuration. In a real-field link deployment, the considered Rx types can tolerate smaller operation depths and can function in shallower waters that those deduced in this work. Thanks to the presented model, one can calculate the noise level for any specific link parameters and solar radiation PSD, and investigate the real impact on the link performance for a given UWOC link deployment scenario. Also, this model can be readily generalized to study the impact of ambient light arising from submarine vehicles' lighting in deep waters. Nevertheless, as a future extension of this work, it is important to investigate a more general link configuration (with respect to the link optical axis and sun position) and to evaluate the precise level of captured solar noise. For such cases, the solar noise power at the Rx is not solely determined by the downwelling plane irradiance and a more general model taking into account the diffused light in water should be considered.

Funding

This work was supported in part by the French PACA (Provence, Alpes, Côte d'Azur) Regional Council and the French Research Institute for Exploitation of the Sea (IFREMER).

Acknowledgment

The authors wish to thank Prof. Hassan Akhouayri and Dr. Frédéric Lemarquis from Institute Fresnel for the fruitful discussions on the practical considerations concerning the transmitter/receiver opto-electronics and solar noise modeling.